Hindawi Publishing Corporation
Mathematical Problems in Engineering
Volume 2012, Article ID 218106, 21 pages
doi:10.1155/2012/218106

Research Article

Control of an Automotive Semi-Active Suspension

Jorge de Jesús Lozoya-Santos, Ruben Morales-Menendez, and Ricardo A. Ramírez Mendoza

Tecnológico de Monterrey, Campus Monterrey, Monterrey, NL, Mexico

Correspondence should be addressed to Jorge de Jesús Lozoya-Santos, jorge.lozoya@itesm.mx

Received 4 March 2012; Accepted 11 April 2012

Academic Editor: Claude Lamarque

Two controllers for an automotive suspensions with Magneto-Rheological (MR) dampers are proposed. One is a model-based using the Linear Parameter Varying (LPV) approach, and the other is a model-free controller with a Frequency Estimation Based (FEB) principle. The LPV controller includes an experimental nonlinear model of an MR damper using only one scheduling parameter. A comparison with a several semi-active controllers for comfort and road holding is discussed. The FEB controller is the best option based on frequency and time response analysis for comfort (10–20%), suspension deflection (30–50%), and road holding (1–5%).

1. Introduction

An MR damper is a nonlinear component used in semi-active suspensions. The accurate modelling of the *force-velocity* curve is not a trivial task due to the hysteresis and nonlinear behavior. These damper features must be included in the controller design. There are several approaches in the control of semi-active suspensions that can be organized as (a) those with experimental validation and (b) those simulation validation. In the first group, the free model controllers such as Sky-Hook (SH), Bolandhemmat et al. [1] and Mix-1-Sensor (M1S), Savaresi and Spelta [2] are more efficient for comfort. Also, the nonlinear control techniques such as model predictive and sliding mode control, Dong et al. [3] and the human simulated intelligent controller, Yu et al. [4] with good experimental results where comfort and road holding are the main goals. In the second group, the H_∞, Choi and Sung [5], using a linear MR damper model and the nonlinear control based on LPV/H_∞, Do et al. [6] have been validated by simulation. These control strategies show several opportunities.

(1) The controller output is not the end damper manipulation, and it is needed because the computation of the desired force of the MR damper or the damping coefficient. This demands a mapping algorithm from control output to manipulation units.

(2) Free-model strategies are more efficient and feasible for implementation than complex controllers.

(3) The antiwindup mechanism is assumed by applying inverse MR damper models, but controllers do not have a feedback of a windup effect.

This paper deals with the (a) design of an LPV controller with one scheduling parameter based on a simple nonlinear MR damper model, (b) design of a free-model controller based on the deflection frequency estimation, and (c) a comparison with several well known comfort, and road-holding controllers. The comparison uses a *quarter of vehicle* (QoV) model and a precise MR damper model. This work is an extended version of Do et al. [7].

This paper is organized as follows. Section 2 reviews the QoV model, different controllers and MR damper models. Section 3 introduces the proposed controllers. Results are presented on Section 4 and discussed in Section 5. Section 6 concludes the paper. Abbreviations and variable definitions are defined in the Nomenclature section.

2. Background

2.1. Passive Nonlinear Suspension Model

The lumped parameter QoV model describes the sprung mass (m_s) corresponding to the vehicle chassis and components, and the unsprung mass (m_{us}); it only captures vertical motions (z_s, z_{us}, $\dot{z}_s$, $\dot{z}_{\text{us}}$, $\ddot{z}_s$, $\ddot{z}_{\text{us}}$). The tire is modeled by a spring linked to the road (z_r) and represented with a stiffness coefficient (k_t), while the tire damping is negligible. A contact point between road and tire always is assumed. The passive suspension, typically modeled by a damper and a spring, exerts vertical resistive forces (F_c, F_{k_s}), Figure 1(a). The vertical force is affected by the square of the motion ratio of damper and spring, (η), Barak [8], and it reflects the projection of the force to the vertical axis in the wheel. A nonlinear passive model will be used as a baseline model ($z \in [\underline{z}, \overline{z}]$ and $\dot{z} \in [\underline{\dot{z}}, \overline{\dot{z}}]$).

$$\begin{aligned} m_s \ddot{z}_s &= -\eta^2 F_{k_s}(z) - \eta^2 F_c(z, \dot{z}, \ddot{z}), \\ m_{\text{us}} \ddot{z}_{\text{us}} &= \eta^2 F_{k_s}(z) + \eta^2 F_c(z, \dot{z}, \ddot{z}) - k_t(z_{\text{us}} - z_r). \end{aligned} \tag{2.1}$$

2.1.1. Performance Objectives

The suspension tuning in automotive applications is used to achieve good comfort, road holding, and safety suspension deflections. These goals demand several industrial specifications in the span of [0–20] Hz, Poussot-Vassal et al. [9].

(i) *Comfort*: the maximum gain of the frequency response $\ddot{z}_s/z_r$ must be kept low, that is <200.

(ii) *Road holding*: the frequency response $(z_{\text{us}} - z_r)/z_r$ ideally must stand closer to 0 (zero).

(iii) *Suspension deflection*: the deflection of the actuator z_{def}/z_r is constrained to preserve the lifetime cycle.

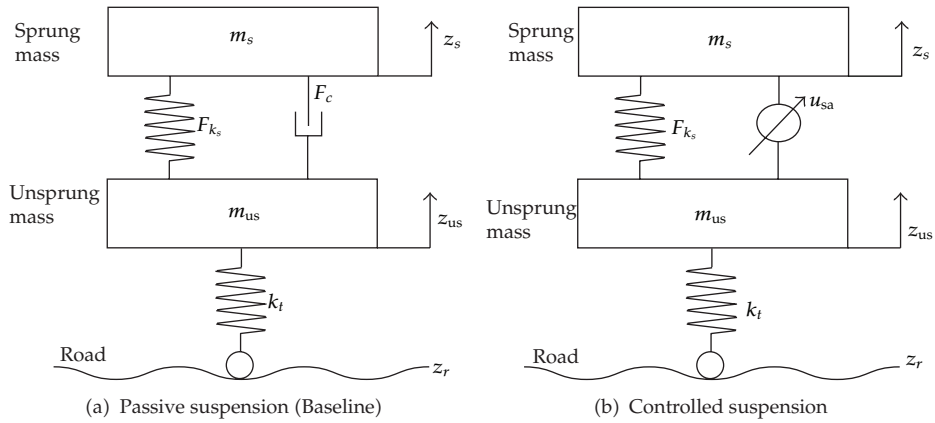

Figure 1: Passive and controlled suspension schemes.

2.2. Controlled Suspension Model

The controlled suspension uses a semi-active damper (F_{MR}) instead of the passive damper (F_c), Figure 1(b). The semi-active damper varies its damping force according to a manipulation (u_{sa}). The QoV model with a controlled suspension is derived as follows ($z \in [\underline{z}, \overline{z}]$ and $\dot{z} \in [\underline{\dot{z}}, \overline{\dot{z}}]$):

$$\begin{aligned} m_s \ddot{z}_s &= -\eta^2 F_{k_s}(z) - \eta^2 F_{MR}(z, \dot{z}, \ddot{z}, u_{sa}), \\ m_{us} \ddot{z}_{us} &= \eta^2 F_{k_s}(z) + \eta^2 F_{MR}(z, \dot{z}, \ddot{z}, u_{sa}) - k_t(z_{us} - z_r), \end{aligned} \tag{2.2}$$

where u_{sa} is the input control of the system provided by the semi-active damper.

2.3. Ideal Damping Ratio

The ideal damping coefficient (c_{ideal}), Miller [10], is computed according to

$$c_{ideal} = 2\sqrt{mk}\ \zeta_{desired}, \tag{2.3}$$

where $2\sqrt{mk}$ is the critical damping for the mass (m), and $\zeta_{desired}$ is the desired damping ratio for a given control strategy. For the sprung mass, $m = m_s$ and $k = k_s$, while for the unsprung mass, $m = m_{us}$ and $k = k_s * k_t/(k_s + k_t)$. An ideal damping force in a QoV suspension is

$$F_{ideal} = c_{ideal}\dot{z}. \tag{2.4}$$

This work uses simulation in the wheel vertical axis, where k_s is surrogated by $k_w = \eta^2 k_s$.

2.4. Benchmark Controllers

Four state-of-the-art controllers were chosen for comparison: Sky Hook (SH) and Mix-1-Sensor (M1S) controllers for comfort, Groundhook (GH) controller for road-holding, and the *Hybrid* controller, which combines the comfort and road holding goals.

2.4.1. SH

The aim of the SH control, Karnopp et al. [11], is to minimize the vertical motion of the sprung mass by connecting a virtual damper between the body and the sky. The adjustable damper is approximated to mimic the virtual damper. The damping force can be represented as

$$F_{\mathrm{SH}} = \begin{cases} c_{\mathrm{SH}}\dot{z}_s, & \text{if } \dot{z}_s(\dot{z}_s - \dot{z}_{\mathrm{us}}) \geq 0, \\ c_{\min}(\dot{z}_s - \dot{z}_{\mathrm{us}}), & \text{if } \dot{z}_s(\dot{z}_s - \dot{z}_{\mathrm{us}}) < 0. \end{cases} \tag{2.5}$$

This technique certainly improves the ride comfort, but it may lead to poor handling. This controller is the reference in comfort due to its practical implementation and design.

2.4.2. M1S

The key principle is the selection of high/low damping at each sampling time to achieve a comfortable ride condition according to the resonance frequency of the QoV, Savaresi and Spelta [2]. It uses only one accelerometer:

$$F_{M1S} = \begin{cases} c_{\max} \cdot \dot{z}, & \text{if } \left(\ddot{z}_s^2 - \alpha^2 \dot{z}_s^2\right) \leq 0, \\ c_{\min} \cdot \dot{z}, & \text{if } \left(\ddot{z}_s^2 - \alpha^2 \dot{z}_s^2\right) > 0. \end{cases} \tag{2.6}$$

M1S has an extensive experimental validation. For a standard automotive suspension, α can be chosen between $[6.3, 12.56]$ rad/s ($[1, 2]$ Hz), according to the resonance frequency of a vertical QoV model.

2.4.3. GH

It uses a fictitious damping element between the wheel and the ground parallel with the tire, Valasek et al. [12]. Equivalent to SH controller, the reduction of dynamic tire-road forces improves the road holding:

$$F_{\mathrm{GH}} = \begin{cases} c_{\mathrm{GH}}\dot{z}_s, & \text{if } -\dot{z}_{\mathrm{us}}(\dot{z}_s - \dot{z}_{\mathrm{us}}) \geq 0, \\ c_{\min}(\dot{z}_s - \dot{z}_{\mathrm{us}}), & \text{if } -\dot{z}_{\mathrm{us}}(\dot{z}_s - \dot{z}_{\mathrm{us}}) < 0. \end{cases} \tag{2.7}$$

The GH control emphasizes the benefits of optimal road holding suspensions.

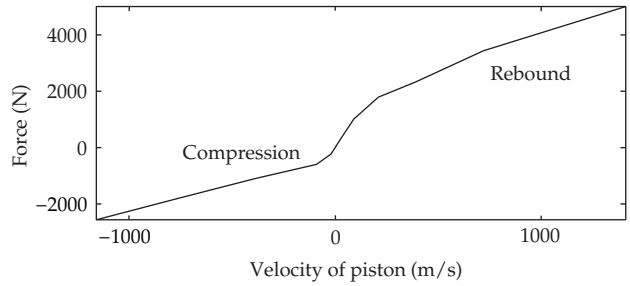

Figure 2: Nonlinear passive damping force used as baseline.

2.4.4. Hybrid

The combination of SH and GH is called hybrid control technique. The corresponding semi-active damping can be expressed as

$$F_{\text{hybrid}} = \beta F_{\text{SH}} + (1-\beta)F_{\text{GH}}, \tag{2.8}$$

where β determines the contribution of SH and/or GH.

2.5. Passive and Semi-Active Dampers

2.5.1. Passive Damper

The passive damper model is the baseline. It is represented by the *force-velocity* curve, Figure 2. It presents a tradeoff for road holding and comfort performances, having a damping force ratio from 3 to 1 between rebound and compression damping zones, Gillespie [13].

2.5.2. Symmetric $V_{\max}$ Model

The nonlinear QoV model with a semi-active suspension is

$$\begin{aligned} F_{\text{MR}} &= k_p z + c_p \dot{z} + m_d \cdot \ddot{z} + f_f \cdot \lambda_{\text{friction}} \\ &\quad c_{\text{MR postyield}} \cdot I \cdot \lambda_{\text{yield}}, \\ \lambda_{\text{friction}} &= \tanh(c_{\text{friction}} \cdot \dot{z} + k_{\text{friction}} \cdot z), \\ \lambda_{\text{yield}} &= \tanh\left(c_{\text{MR preyield}} \cdot \dot{z} + k_{\text{MR postyield}} \cdot z\right). \end{aligned} \tag{2.9}$$

The MR damper model (2.9) includes the friction, preyield, and postyield operating modes.

2.5.3. Asymmetric Full Modified SP Model

The model describes a passive linear damping and stiffness coefficients and it includes a lineal varying damping of the preyield and postyield modes of operation of the MR fluid using a receding horizon computed from the velocity of piston

$$F_{\mathrm{MR}} = c_{\mathrm{MR}} \cdot I \cdot \rho + c_p \dot{z} + k_p z. \tag{2.10}$$

The model (2.10) includes the nonlinearities of the MR damper with the parameters

$$\begin{aligned} \rho &= \frac{\dot{z}}{\dot{z}_\infty}, \quad \rho \in [-1, 1], \\ \dot{z}_\infty &= \|(|\dot{z}|)\|_{\infty_{i-k}}^{i} = \sup\{\dot{z}_{i-k} \cdots \dot{z}_i\}. \end{aligned} \tag{2.11}$$

3. Proposed Controllers

3.1. LPV Controller

The representation of a QoV in the LPV framework ($F_{dz} = 0$ and $D = 0$) is as follows:

$$\begin{bmatrix} \dot{z}_s \\ \ddot{z}_s \\ \dot{z}_{\mathrm{us}} \\ \ddot{z}_{\mathrm{us}} \end{bmatrix} = A_s \begin{bmatrix} z_s \\ \dot{z}_s \\ z_{\mathrm{us}} \\ \dot{z}_{\mathrm{us}} \end{bmatrix} + \begin{bmatrix} B_s & B_{s1} \end{bmatrix} \begin{bmatrix} u_c \\ z_r \end{bmatrix}, \qquad y = C_s \begin{bmatrix} z_s \\ \dot{z}_s \\ z_{\mathrm{us}} \\ \dot{z}_{\mathrm{us}} \end{bmatrix},$$

$$A_s = \begin{bmatrix} 0 & 1 & 0 & 0 \\ \dfrac{-k_s - k_p}{m_s} & -\dfrac{c_p}{m_s} & \dfrac{k_s + k_p}{m_s} & \dfrac{c_p}{m_s} \\ 0 & 0 & 0 & 1 \\ \dfrac{k_s + k_p}{m_{\mathrm{us}}} & \dfrac{c_p}{m_{\mathrm{us}}} & \dfrac{-k_s - k_p - k_t}{m_{\mathrm{us}}} & -\dfrac{c_p}{m_{\mathrm{us}}} \end{bmatrix}, \tag{3.1}$$

$$B_s = \begin{bmatrix} 0 \\ -\dfrac{c_{\mathrm{MR}} \cdot \rho_{\mathrm{sat}}}{m_s} \\ 0 \\ \dfrac{c_{\mathrm{MR}} \cdot \rho_{\mathrm{sat}}}{m_{\mathrm{us}}} \end{bmatrix}, \qquad B_{s1} = \begin{bmatrix} 0 \\ 0 \\ 0 \\ \dfrac{k_t}{m_{\mathrm{us}}} \end{bmatrix}, \qquad C_s = \begin{bmatrix} 0 \\ 1 \\ 0 \\ -1 \end{bmatrix}^T,$$

where $u_c = u_{\mathrm{sa}}$. The input constraints are as follows:

(1) Semiactiveness

The input of the damper model will be positive

$$u_{\mathrm{sa}} = |u_c|, \tag{3.2}$$

where u_c is the LPV controller output.

(2) Saturation

The control input provided by the semi-active damper has a finite interval $[0, I_{\max}]$ A. A new measurable parameter is introduced in order to bound the electric current I into the damper as follows:

$$\rho_{\text{sat}} = \left[\frac{\tanh\left[(I\rho)/(I_{\max}\cdot\rho)\right]}{(I\rho)/(I_{\max}\cdot\rho)}\right], \quad \rho_{\text{sat}} \in [0,1], \tag{3.3}$$

where $I\rho$ is the term modifying the MR damping coefficient c_{MR} according to the velocity of piston. A new parameter $\rho^* = \rho\rho_{\text{sat}}$ is substituted in (2.10):

$$F_{\text{MR}} = c_{\text{MR}}\cdot I\cdot\rho^* + c_p\dot{z} + k_p z. \tag{3.4}$$

Simplifying (3.4) with $\tanh(v) = \text{sign}(v)\tanh(|v|)$, and substituting $\rho = |\dot{z}|/\dot{z}_\infty$:

$$F_{\text{MR}} = c_{\text{MR}}\cdot\rho\cdot I_{\text{sat}} + c_p\dot{z} + k_p z, \tag{3.5}$$

$$I_{\text{sat}} = I_{\max}\ \tanh\left[\frac{I}{I_{\max}}\right], \quad I_{\text{sat}} \in [0, I_{\max}], \tag{3.6}$$

where $I = u_{\text{sa}}$ and limited to to $I_{\max}$. I_{sat} is the applied electric current to the suspension.

(3) Dissipativity

The damping coefficient always must be positive. The term of (3.5), which depends on I_{sat} is simplified by substituting $\rho = |\dot{z}|/\dot{z}_\infty$:

$$F_{d,\text{MR}} = c_{\text{MR}}\cdot I_{\text{sat}}\cdot\rho = c_{\text{MR}}\cdot I\cdot\frac{\dot{z}}{\dot{z}_\infty}. \tag{3.7}$$

Dividing by $\dot{z}$, the damping coefficient due to I is

$$c_{d,\text{MR}} = \frac{F_{d,\text{MR}}}{\dot{z}} = \frac{c_{\text{MR}}}{\dot{z}_\infty}\cdot I_{\text{sat}}, \tag{3.8}$$

where $c_{d,\text{MR}}$ is the MR damping coefficient due to the electric current changes. It can be concluded that $c_{d,\text{MR}}$: (a) is always positive, (b) it is proportional to I_{sat}, and (c) it is inversely proportional to the maximum velocity, that is, low velocities will amplify the damping coefficient and vice versa.

3.1.1. LPV Controller Design

The generalized system for the H_∞/LPV controller synthesis for one scheduling parameter considers a filter in the input of LPV system (3.1) to be proper for the LPV synthesis. ρ^* will

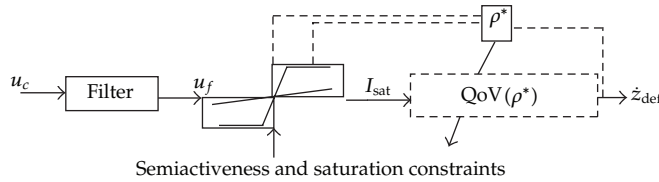

Figure 3: Model with a semi-active bounded input saturation.

Table 1: Parameters for H_∞/LPV semi-active suspension design.

		$W_{\ddot{z}_s}$			W_{filter}
Ω_{11}	Ω_{12}	ξ_{11}	ξ_{12}	$k_{\ddot{z}_s}$	Ω_f
33.29	28.54	52.32	5.26	1.95	51.1
		$W_{(z_{\text{us}}-z_r)}$			W_{z_r}
Ω_{21}	Ω_{22}	ξ_{21}	ξ_{22}	$k_{(z_{\text{us}}-z_r)}$	Constant
1.29	0.072	4.09	0.136	0.152	7×10^{-2}

be in the states transition matrix A, Do et al. [6]. Figure 3 shows the QoV model using the MR damper with saturated input.

To meet the control specifications, two H_∞ weighting functions ($W_{\ddot{z}_s}$ and $W_{z_{\text{us}}-z_r}$), were used according to the comfort performance without affecting the road holding, Do et al. [14].

$$
\begin{aligned}
W_{\ddot{z}} &= k_{\ddot{z}_s} \frac{\Omega_{11}^2 + 2\xi_{11}\Omega_{11}s + s^2}{\Omega_{12}^2 + 2\xi_{12}\Omega_{12}s + s^2}, \\
W_{z_{us}-z_r} &= k_{z_{\text{us}}-z_r} \frac{\Omega_{21}^2 + 2\xi_{21}\Omega_{21}s + s^2}{\Omega_{22}^2 + 2\xi_{22}\Omega_{22}s + s^2}, \\
W_{\text{filter}} &= \frac{\Omega_f}{s + \Omega_f}, \qquad W_{z_r} = 7 \times 10^{-2}.
\end{aligned}
\tag{3.9}
$$

The LPV controller was synthesized using the *SeDuMi Matlab* toolbox. The controlled output vector is $z = (\ddot{z}_s, z_{\text{us}})^T$, Figure 4. Table 1 shows the parameters for H_∞/LPV semi-active suspension design.

3.2. FEB Controller

By assuming a harmonic motion ($z \sim R \cdot \sin(\omega \cdot t)$) of the damper piston, the state variables of the system are

$$
\begin{aligned}
\dot{z} &\sim \omega \cdot R \cdot \cos(\omega \cdot t), \\
\ddot{z} &\sim -(\omega)^2 \cdot R \cdot \sin(\omega \cdot t).
\end{aligned}
\tag{3.10}
$$

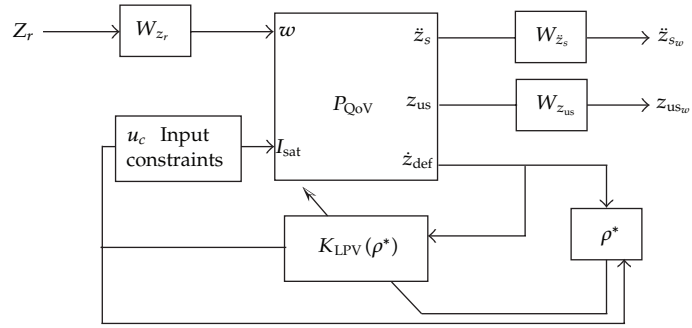

Figure 4: LPV-based controller.

The signals z and $\dot{z}$ are unknown. Using the *root mean square* (RMS) of deflection and velocity deflection of the MR damper piston, an approximation is:

$$R \sim z_{\mathrm{rms}} \cdot \sqrt{2}, \tag{3.11}$$

$$\omega \cdot R \sim \dot{z}_{\mathrm{rms}} \cdot \sqrt{2}. \tag{3.12}$$

Substituting (3.11) in (3.12), and $\omega = 2 \cdot \pi \cdot f$:

$$2 \cdot \pi \cdot f \cdot z_{\mathrm{rms}} \cdot \sqrt{2} \sim \dot{z}_{\mathrm{rms}} \cdot \sqrt{2}. \tag{3.13}$$

The estimation of the frequency is

$$\widehat{f} = \frac{(\dot{z}_{\mathrm{rms}})}{(2 \cdot \pi \cdot z_{\mathrm{rms}})}. \tag{3.14}$$

The formula for a continuous function $y(t)$ for the RMS over the interval of time $T_1 \le t \le T_2$ is

$$y_{\mathrm{rms}} = \sqrt{\frac{1}{T_2 - T_1} \cdot \int_{T_1}^{T_2} \left[y(t)\right]^2 dt}. \tag{3.15}$$

A numerical integration computes the discrete RMS value

$$y_{\mathrm{rms}} = \sqrt{\frac{y_1^2 + y_2^2 + \cdots + y_n^2}{n}}. \tag{3.16}$$

Substituting (3.16) in (3.14):

$$\widehat{f} = \sqrt{\frac{\left(\dot{z}_1^2 + \dot{z}_2^2 + \cdots + \dot{z}_n^2\right)}{\left(z_1^2 + z_2^2 + \cdots + z_n^2\right) \cdot 4\pi^2}}. \tag{3.17}$$

Table 2: Look-up table for selection of electrical current based on frequency estimation.

$\widehat{f}(=)$Hz	BW_1	BW_2	BW_3	BW_4
$I(=)$A	I_1	I_2	I_3	I_4

Table 3: Parameters model.

Symmetric V_{max} model					
c_p	k_p	c_{MR}		receding horizon_k	
1061	−1307	401		128 samples	
Asymmetric full modified SP model					
Parameters for $\dot{z} > 0$					
c_p	k_p	m_{damper}	f_f	$c_{preyield}$	$k_{preyield}$
607	5370	4	127	398	90
$c_{MR\ postyield}$		$c_{MR\ preyield}$		$k_{MR\ preyield}$	
441		7.8		−20	
Parameters for $\dot{z} < 0$					
c_p	k_p	m_{damper}	f_f	$c_{preyield}$	$k_{preyield}$
604	−2836	4.2	128	530	265
$c_{MR\ postyield}$		$c_{MR\ preyield}$		$k_{MR\ preyield}$	
421		7.4		1.2	

Cartwright [15] states n that defines the RMS. The chosen frequencies were 2 and 14 Hz. Using the frequency estimation and observing the pseudo-Bodes of the variables, the look-up table was defined to assure the desired performances, Table 2.

4. Results

4.1. Identification of MR Damper Models

The experimental training path for identification is a sinusoidal with variable amplitude ±8 mm and frequency of 7 Hz. The amplitude randomly varies each 3 cycles. The electric current is a *Random Walk*, Ljung [16], with a span of 0–2.5 A. The spans of $\dot{z}$ and f_{MR} were $\mp 0.6\,\text{m/s}$ and $\mp 2,500\,\text{N}$, Lozoya-santos et al. [17]. The experimental data for model learning consist of four datasets. Three datasets with N series of three periods of a sinusoidal, where the amplitude is constant. Each dataset explores $N = 29$ frequencies, $f_i = \{0.5, 1, 14.5\}$ Hz with $I = \{0, 1.25, 2.5\}$ A. The fourth dataset is a *Road Profile* with fluctuant electric current. The identified models are shown in Table 3. The *Error-to-Signal Ratio* (ESR) index, Savaresi et al. [18], was exploited for model validation, Table 4. A qualitative validation was the analysis of the *force-velocity* plots of the MR damper, Figure 5.

4.2. QoV Lumped Parameters

The lumped parameters of the QoV have been taken from a commercial vehicle model, Table 5.

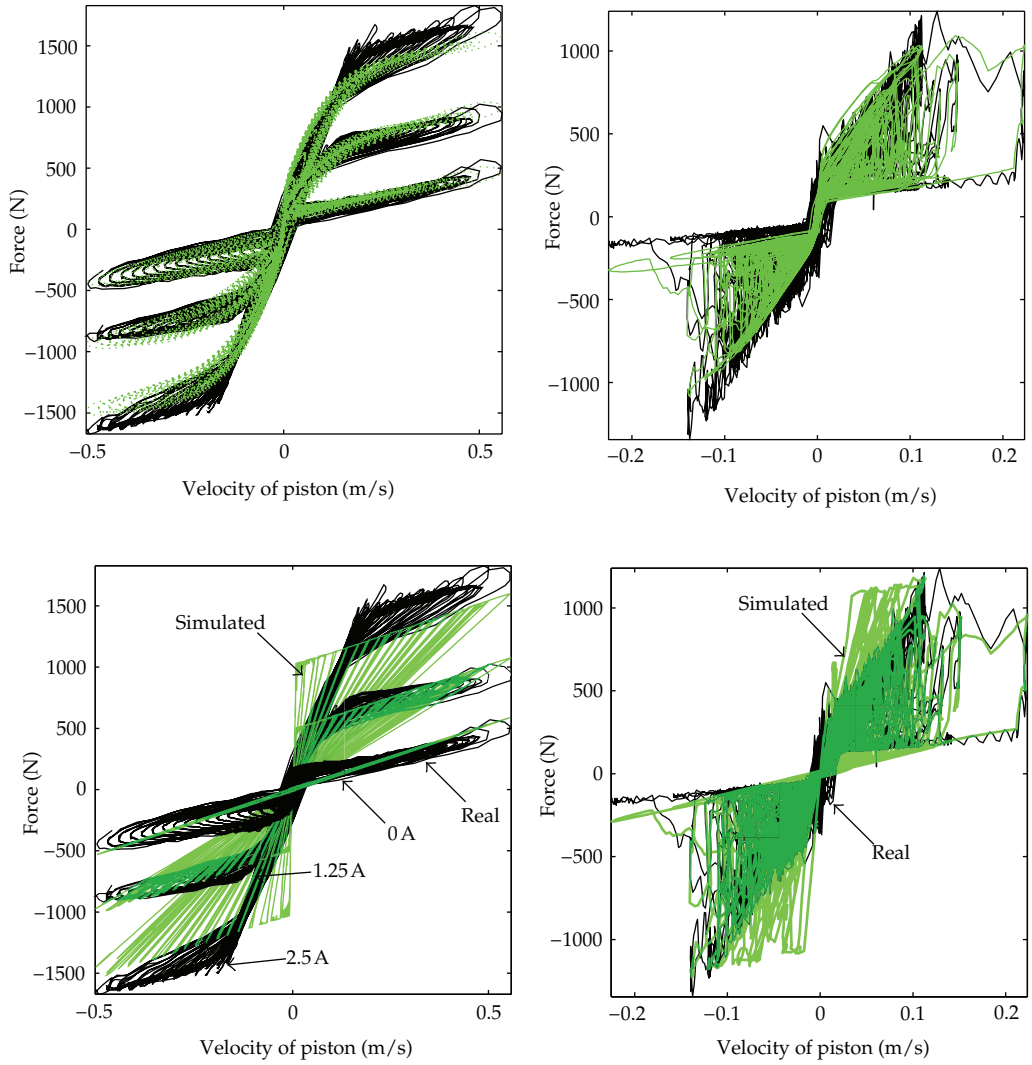

Figure 5: Top plots correspond to the full modified SP model, and bottom to V_{max} model. Left plots show feature of constant electric current and *Chirp* signal, right are for fluctuant electric current and Road Profile.

Table 4: ESR index for MR damper models.

Step	Learning	Testing			
Experiment	1	1	2	3	4
Full model SP	0.031	0.016	0.013	0.025	0.073
V_{max}	0.089	0.211	0.247	0.123	0.194

4.3. Semi-Active Force Tracking

The values of c_{SH}, c_{GH}, c_{min},and c_{max} are computed according to the ideal damping ratio for on/off semi-active systems, Miller [10]. The degrees of freedom α in M1S, and β for hybrid control are defined $2.2 \cdot 2 \cdot \pi$ and 0.5, respectively. Table 6 shows the ideal damping coefficients.

Table 5: QoV parameters.

Component of the QoV	Value	Units
Sprung mass (m_s)	522	Kg
Unsprung mass (m_{us})	50	Kg
Spring stiffness (k_s)	83	kN/m
Tire stiffness (k_t)	230	kN/m
Suspension stroke	[0.05, −0.07]	m
Suspension maximum velocity	[1.2, −1.5]	m/s
Motion ratio η	0.614	—
m_s resonance frequency (f_{m_s})	1.2	Hz
m_{us} resonance frequency ($f_{m_{\text{us}}}$)	11.5	Hz

Table 6: Damping coefficients.

Damping	ζ	m	k	c_{ideal} [Ns/m]
c_{SH}	0.6	m_s	$\eta^2 k_s$	4,826
c_{M1S}	0.6	m_s	$\eta^2 k_s$	7,225
$c_{\text{min}_{\text{SH}}}$	0.15	m_s	$\eta^2 k_s$	1,207
$c_{\text{min}_{\text{M1S}}}$	0.05	m_s	$\eta^2 k_s$	1,084
c_{GH}	1	m_{us}	$(\eta^2 k_s * k_t)/(\eta^2 k_s + k_t)$	4,826
$c_{\text{min}_{\text{road}}}$	0.15	m_{us}	$(\eta^2 k_s * k_t)/(\eta^2 k_s + k_t)$	1,206

Since the benchmark controllers output has *Newton* units, a feedback control system is included, Figure 6(a). A PI controller is considered, Lee and Choi [19]. The output of the controllers has ampere units, there was not necessary a feedback control, Figure 6.

4.4. Frequency Domain Tests

The evaluation of the QoV model was done in open- and close-control systems based on industrial specifications, Sammier et al. [20] and realistic road tests, Boggs et al. [21]. According to these bandwidths, a road profile is designed based on the shape of the relative amplitude spectrum of the position command at 10 points between 0.1 and 20 Hz. This shape does not introduce unrealistic velocities into the shock absorber, Boggs et al. [22]. The amplitude relative is 15 mm according to the several manoeuvres in a real vehicle suspension, Fukushima et al. [23]. The qualitative comparison of the frequency responses uses the *Variance Gain* algorithm, Savaresi et al. [24]. The power spectral density (PSD) allows a quantitative comparison, Poussot-Vassal et al. [9]. A negative percentage means the uncontrolled suspension is better in the given frequencies of interest.

4.4.1. Open-Control System

Six open-control system simulations with $I = \{0, 0.5, 1.25, 2.5, 3, 5\}$ A without taking into account the motion ratio. These frequency responses allow to observe the optimal cases of the uncontrolled suspension for comfort (0 A), road holding (5 A), and a tradeoff damping (2.5 A), Figure 7.

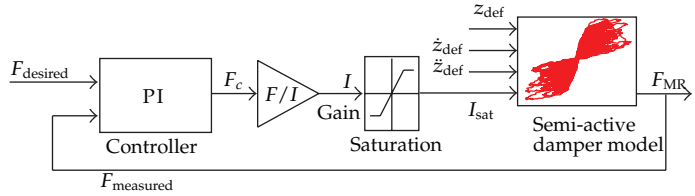

(a) Control strategy for changing force to electric current. The strategy acts on a nonlinear MR damper model

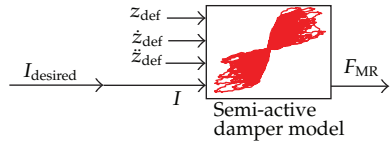

(b) Output of the proposed controller is the input of the nonlinear MR damper model

Figure 6: Control schemes.

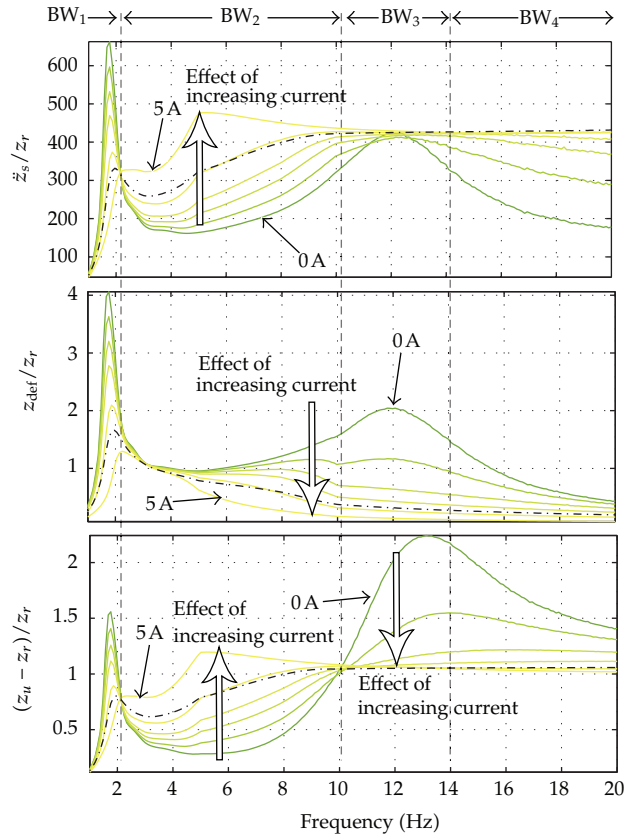

Figure 7: Open-control system. Pseudo-Bode of: $\ddot{z}_s/z_r$, z/z_r, and $(z_{\text{us}} - z_r)/z_r$. The arrows show the gain increasing direction because of the applied electric current.

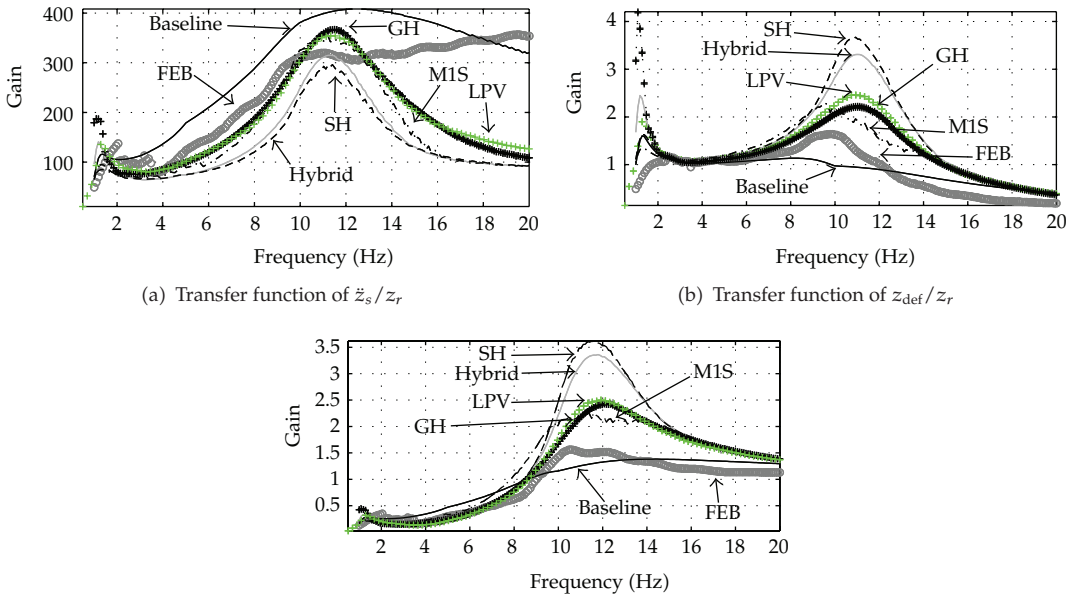

(a) Transfer function of $\ddot{z}_s/z_r$

(b) Transfer function of z_{def}/z_r

(c) Transfer function of $(z_{\text{us}} - z_r)/z_r$

Figure 8: Control system. Pseudo-Bodes for transfer functions (a) sprung-mass acceleration, (b) suspension deflection, and (c) road holding versus road profile.

4.4.2. Control System

Six control system simulations, each one with the control strategies SH, GH, Hybrid, M1S, FEB, and LPV were compared, Figure 8.

Figure 9 shows the improved percentages of PSD each control system.

4.5. Time Domain Tests

Ride comfort and road holding normally occurs in 1-2 Hz and 10–15 Hz. Figure 10 compares the uncontrolled and controlled suspensions in the body and road holding resonance. These comparisons show the benefit of the LPV and FEB controllers. The resonance frequencies are shown in Table 5. The amplitudes of the sinusoidal tests were ±10 mm and ±1 mm. Also, the RMS of each signal are shown. The improved percentage of RMS validates the benefit of using a controlled suspension. A negative RMS indicates the uncontrolled suspension has better performance. The exerted electric currents I for the proposed controllers and the best controllers for comfort and road holding are shown in Figure 11, and the improved percentages of RMS in Figure 12.

5. Discussion

5.1. Frequency Domain

5.1.1. Open-Control System

The comfort condition depends on $\ddot{z}_s/z_r$, Figure 7 (upper plot). In bandwidth 1 (BW_1, 0–2 Hz), a comfort condition and good handling are achieved with $I > 1$ A (i.e., gain < 200),

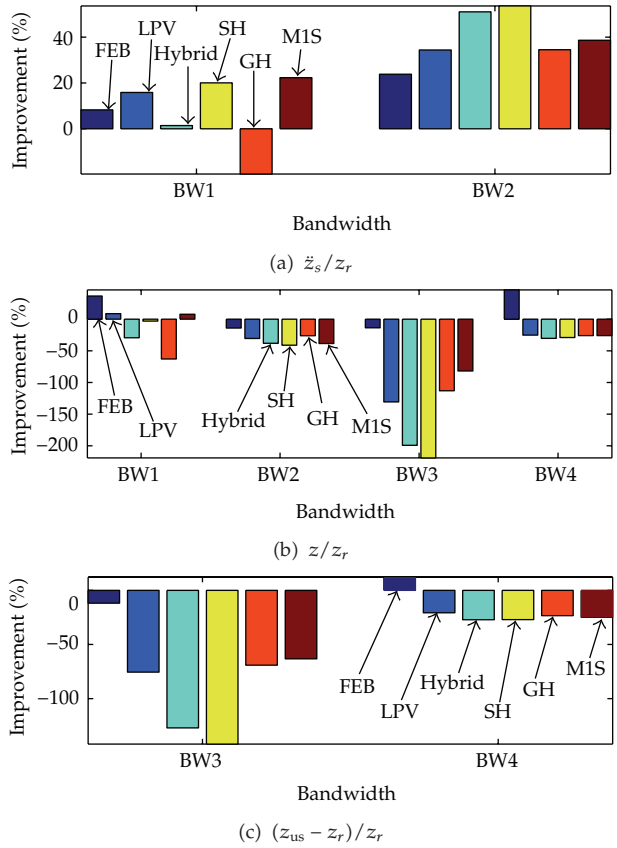

Figure 9: Improved percentages of PSD for (a) sprung-mass acceleration transfer function in comfort bandwidths, (b) suspension deflection in all bandwidths, and (c) tire deflection in road holding bandwidths.

and with $I \sim 0$ A in bandwidth 2 (BW_2, 2–10 Hz). In bandwidth 4 (BW_4, 14–20 Hz), actuation is needed to kept the comfort condition. For bandwidth 3 (BW_3, 10–14 Hz), due to the tire-hop frequency, the applied $I > 2.5$ A decreases the gain in $\ddot{z}$.

The suspension deflection transfer function improves by holding higher current below 2 Hz and between 5–20 Hz. In the span from 2–5 Hz and 16–20 Hz, the electric current has not influence on this performance, Figure 7 (middle plot).

Transfer functions $(z_{us} - z_r)/z_r$ are associated with the road holding, Figure 7 (lower plot). In BW_1, 2.5 A meets the industrial specifications, (included the comfort conditions). In BW_2, 0 A keeps a low gain close to zero, comfort condition shares these electric currents in later frequency spans. Over 10 Hz, a difference from comfort condition, 2.5 A is desirable to allow the road holding. Table 7 summarizes the optimal electric currents.

5.1.2. Control System

Comfort

The baseline suspension is not optimized for comfort (i.e., it is a hard suspension) see Figure 8(a). The SH and the hybrid controllers offer excellent performances with the lowest

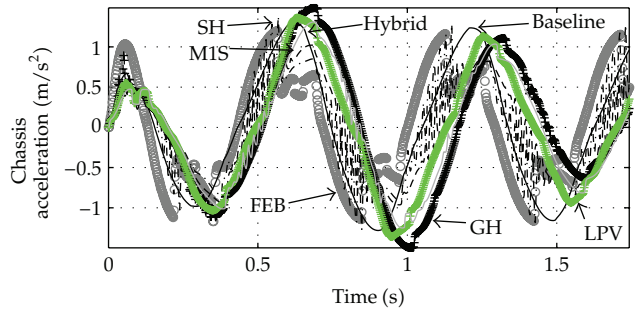

(a) $\ddot{z}_s(t)$ under f_{m_s}

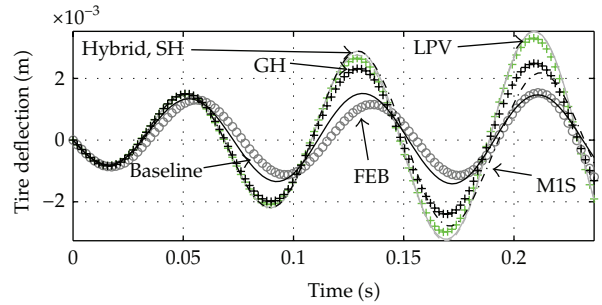

(b) $(z_{\text{us}} - z_s)/z_r(t)$ under $f_{m_{\text{us}}}$

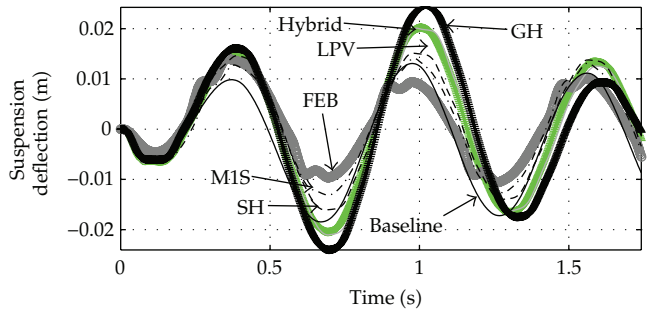

(c) $z_{\text{def}}(t)$ under f_{m_s}

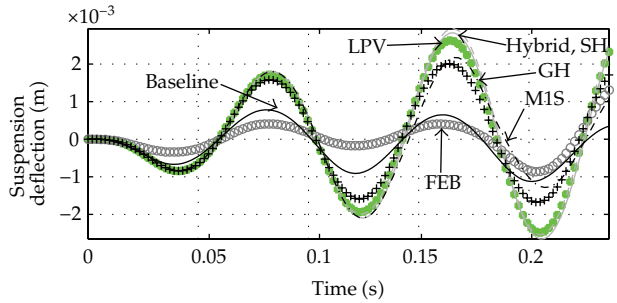

(d) $z_{\text{def}}(t)$ under $f_{m_{\text{us}}}$

Figure 10: Transient response for (a) sprung-mass acceleration at f_{m_s}, (b) tire deflection at $f_{m_{\text{us}}}$, and ((c), (d)) suspension deflection under resonance frequencies.

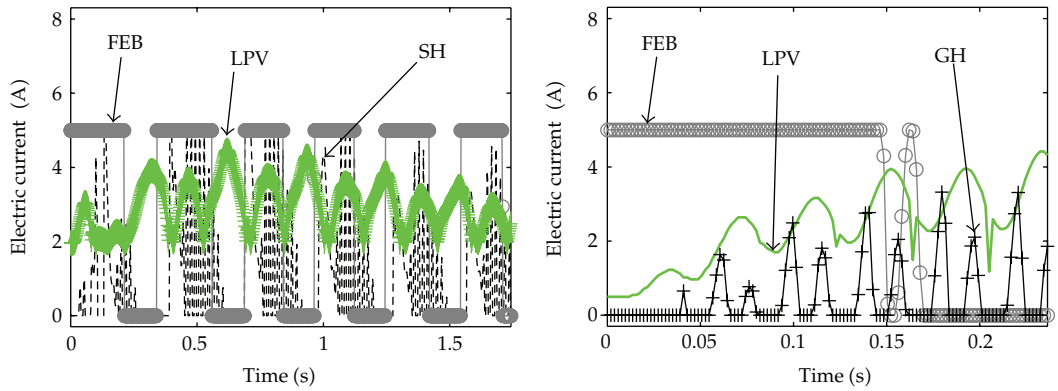

(a) I under f_{m_s} (b) I under $f_{m_{us}}$

Figure 11: Electric current of transient response for a sinusoidal road under resonance frequencies oscillation.

Table 7: Look-up table for the best performance in comfort and road holding.

$\hat{f}(=)$Hz	0–2	2–12	12–14	14–20
$I(=)$A	2.5	0	2.5	0

gains, $\ddot{z}_s$, in $[4, 20]$ Hz. Below 4 Hz, the best case is not clear with exception of the baseline suspension and GH controller both being the worst controllers.

Suspension Deflection

The best controllers are FEB and M1S, Figure 8(b). The baseline suspension presents the better suspension deflection. The worst controllers are the SH and hybrid. All the controllers present similar performances in the (3–7) Hz span, Figure 8(b).

Road Holding

The best performance corresponds to the baseline suspension. The best controller is the FEB. The M1S, GH, and LPV have similar performances. The SH and hybrid are not well suited, Figure 8(c).

The hybrid does not achieve a good performance for comfort/road holding. The baseline suspension is optimized for suspension deflection and road holding. The controller with the best tradeoff is the FEB.

The proposed controllers have an improved performance of 10% and 17% in the primary ride frequencies (BW1), while the SH and M1S are the best (20% and 22%), Figure 7(a). In secondary ride (BW2), all the controllers have improved results. In suspension deflection, FEB and LPV-based exhibit better results, Figure 7(a). In general, the benchmark controllers are not well suited for improvement of suspension deflection. Results for road holding support FEB controller as the best one. The LPV-based controller equals GH controller. The frequency domain analysis validates FEB and LPV as the best options for both comfort and road holding.

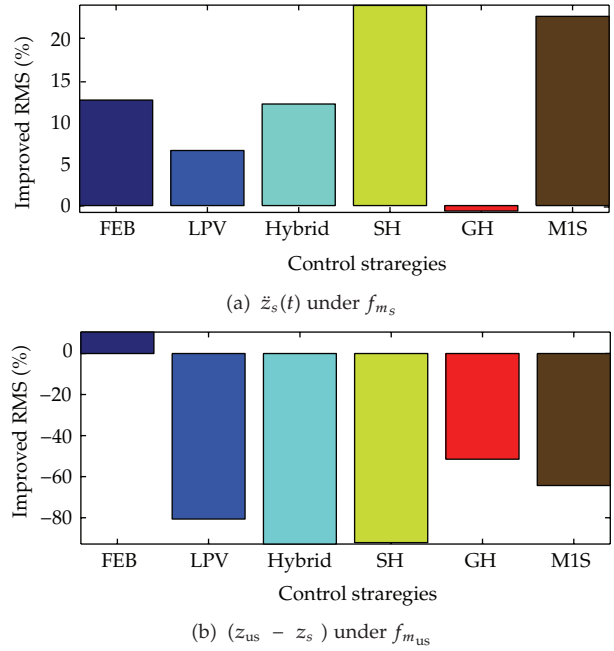

(a) $\ddot{z}_s(t)$ under f_{m_s}

(b) $(z_{\text{us}} - z_s)$ under $f_{m_{\text{us}}}$

Figure 12: Improved RMS in transient response for (a) sprung-mass acceleration at f_{m_s}, and (b) tire deflection at $f_{m_{\text{us}}}$, under resonance frequencies.

5.2. *Transient Response*

The FEB controller shows optimum performances for sprung-mass acceleration, Figure 10(a), and tire deflection, Figure 10(b). The rest of the controllers have similar performances, but the SH is the best in comfort, Figure 10(a). The FEB controller achieves a safe deflection while the other controllers have low performances Figures 10(c) and 10(d).

Dissipativity Constraint

The FEB controller uses two damping coefficients, related to $I = \{0, 2.5\}$ A, for low and high damping. Its design avoids saturation problem. The LPV controller, includes the saturation in the scheduling parameter. Figures 11(a) and 11(b) show how a valid manipulation according to the dissipativity constraint is obtained. Figures 11(a) and 11(b) also show the manipulation of the classical SH and GH controllers that have higher frequency content.

Results show how the FEB controller obtains the comfort and road holding, while the hybrid controller does not achieve the minimum compromise. Also, the FEB controller follows the performance of SH and M1S in comfort (Figure 12(a)) of GH controller in road holding, Figure 12(b). A main contribution of the LPV controller is the use of only one scheduling parameter, Do et al. [7].

6. Conclusion

Two controllers for an automotive suspension with Magneto-Rheological (MR) dampers are proposed: one is based on the model using Linear Parameter-Varying (LPV) approach, and

the other is a free of model using a frequency estimation of the road profile. A comparison with several semi-active control strategies for comfort and road holding was presented. Both controllers exhibit important features for practical applications: (1) the controller output is the electric current through MR damper coil, (2) the controllers achieve the objectives with a bounded output, (3) the scheduling parameter is based on one measurement, (4) there is no real-time computation of derivatives of matrix, hence the controllers allow good sampling time, (5) the LPV controller is linear combination of matrices, and the FEB computes the 1-norm of two signals over n samples, and (6) the controllers can modify their goal performances with a set of matrices for LPV, and a look-up table of electric current for (FEB).

Nomenclature

c_{MR}:	MR damping coefficient $((\mathrm{N}\cdot\mathrm{A})/\mathrm{m})$
$c_{d,\mathrm{MR}}$:	Applied MR damping coefficient $((\mathrm{N}\cdot\mathrm{A})/\mathrm{m})$
$c_{\max}, c_{\min}$:	Max/Min damping coefficient (Ns/m)
c_p:	Passive damping coefficient (Ns/m)
$c_{\mathrm{SH}}, c_{\mathrm{GH}}$:	Skyhook/groundhook coefficient (Ns/m)
c_{friction}:	Gain of f_f due to $\dot{z}$ (s/m)
k_{friction}:	Gain of f_f due to z (1/m)
$c_{\mathrm{MR\ preyield}}$:	Preyield damping gain (s/m)
$c_{\mathrm{MR\ postyield}}$:	Postyield damping (N/A)
$k_{\mathrm{MR\ preyield}}$:	Preyield gain due to stiffness (1/m)
m_d:	Virtual mass of the MR damper (kg)
$\widehat{f}$:	Estimated frequency by FEB controller (Hz)
k_p:	Internal stiffness coefficient (N/m)
k:	Receding horizon in order to compute $\|\|\|\dot{z}\|\|\|_\infty$
u_{sa}:	Determines the damping coefficient magnitude when the device is in tension or compression
w:	Perturbation shaped as chirp sinusoidal
z, z_{def}:	Piston deflection (m)
$\dot{z}, \dot{z}_{\mathrm{def}}$:	Piston deflection velocity (m/s)
$\dot{z}_{\min}, \dot{z}_{\max}$:	Minimum/maximum measured $\dot{z}$
$\ddot{z}$:	Piston deflection acceleration ($\mathrm{m/s^2}$)
$\dot{z}_s, \ddot{z}_s$:	Sprung mass velocity, acceleration (m/s, $\mathrm{m/s^2}$)
z_{us}:	Unsprung mass displacement (m)
$\dot{z}_{\mathrm{us}}, \ddot{z}_{\mathrm{us}}$:	Unsprung mass velocity, acc (m/s, $\mathrm{m/s^2}$)
$\overline{z}, \overline{\dot{z}}, \underline{z}, \underline{\dot{z}}$:	Upper/lower limits in suspension $(\mathrm{m}, \mathrm{m/s^2})$
A_s, B_s, B_{s1}, C_s, D:	Matrices of state space representation according to Do et al. [7]
BW_j:	j-esime bandwidth in FEB control
$I, I_{\max}, I_{\mathrm{sat}}$:	Electric current, maximum I, bounded I (A)
F_c, F_{dz}:	Vertical damper, steering force (N)
F_{k_s}:	Vertical spring force (N)
F_{MR}:	MR damping force (N)
$F_{d,\mathrm{MR}}$:	MR damping force (N) due to I fluctuations

F_{SH}, F_{GH}: Skyhook, groundhook force (N)
F_{M1S}, F_{hybrid}: Mixed-1-sensor, hybrid Force (N)
R: Sinusoidal amplitude (m)
$W_{z_r}, W_{z_s}, W_{z_{us}}$: Weighting function road profile, sprung-mass acceleration, unsprung-mass displacement
$|||\dot{z}|||_\infty$: Absolute maximum deflection velocity, $\dot{z}_\infty : \{\|(|\dot{z}|)\|^i_{\infty_{i-k}} \in [\dot{z}_{\min}, \dot{z}_{\max}]\}$
η: Motion ratio in wheel axis
β: Tradeoff parameter for comfort/road holding
ρ: Effect of the mechanical and hydraulic properties of the damper on c_{MR}
ρ_{sa}: Semiactiveness of the LPV output controller
ρ_{sat}: Dynamic saturation of the electric current limited to a maximum value I_{max} and ρ
ρ^*: Scheduling parameter for LPV controller
ω: Frequency (rad/s).

Acknowledgments

Authors thank the PCP 06/2007 program (CONACyT) and Autotronics Research Chair (Tecnologico de Monterrey).

References

[1] H. Bolandhemmat, C. M. Clark, and F. Golnaraghi, "Development of a systematic and practical methodology for the design of vehicles semi-active suspension control system," *Vehicle System Dynamics*, vol. 48, no. 5, pp. 567–585, 2010.
[2] S. M. Savaresi and C. Spelta, "A single-sensor control strategy for semi-active suspensions," *IEEE Transactions on Control Systems Technology*, vol. 17, no. 1, pp. 143–152, 2009.
[3] X. M. Dong, M. Yu, C. R. Liao, and W. M. Chen, "Comparative research on semi-active control strategies for magneto-rheological suspension," *Nonlinear Dynamics*, vol. 59, no. 3, pp. 433–453, 2010.
[4] M. Yu, X. M. Dong, S. B. Choi, and C. R. Liao, "Human simulated intelligent control of vehicle suspension system with *MR* dampers," *Journal of Sound and Vibration*, vol. 319, no. 3–5, pp. 753–767, 2009.
[5] S. B. Choi and K. G. Sung, "Vibration control of magnetorheological damper system subjected to parameter variations," *International Journal of Vehicle Design*, vol. 46, no. 1, pp. 94–110, 2008.
[6] A. L. Do, O. Sename, and L. Dugard, "An *LPV* control approach for semi-active suspension control with actuator constraints," in *Proceedings of the American Control Conference (ACC '10)*, pp. 4653–4658, Baltimore, Md, USA, July 2010.
[7] A. L. Do, O. Sename, L. Dugard, and R. Ramirez, "An *LPV* approach for semi-active suspension control," in *Proceedings of the 11th Pan-American Congress of Applied Mechanics*, Paraná, Brazil, 2010.
[8] P. Barak, "Magic numbers in design of suspensions for passenger cars," SAE Technical Paper 911921, 1991.
[9] C. Poussot-Vassal, O. Sename, L. Dugard, P. Gáspár, Z. Szabó, and J. Bokor, "A new semi-active suspension control strategy through *LPV* technique," *Control Engineering Practice*, vol. 16, no. 12, pp. 1519–1534, 2008.
[10] L. R. Miller, "Tuning passive, semi-active, and fully active suspension systems," in *Proceedings of the 27th IEEE Conference on Decision and Control*, pp. 2047–2053, December 1988.
[11] D. Karnopp, M. J. Crosby, and R. A. Harwood, "Vibration control using semi-active force generators," *Journal of Engineering for Industry*, vol. 96, no. 2, pp. 619–626, 1974.

[12] M. Valasek, M. Novak, Z. Sika, and O. Vaculin, "Extended ground-hook—new concept of semi-active control of truck suspension," *Vehicle System Dynamics*, vol. 29, pp. 289–303, 1997.
[13] T. D. Gillespie, *Fundamentals of Vehicle Dynamics*, SAE International, Washington, DC, USA, 1992.
[14] A. L. Do, B. Soualmi, J. Lozoya-Santos, O. Sename, L. Dugard, and R. Ramirez, "Optimization of weighting function selection for H_∞ control of semi-active suspensions," in *Proceedings of the 12th Mini Conference on Vehicle System Dynamics, Identification and Anomalies*, Budapest, Hungary, 2010.
[15] K. V. Cartwright, "Determining the effective or RMS voltage or various waveforms without calculus," *The Technology Interface*, vol. 8, no. 1, pp. 1–20, 2007.
[16] L. Ljung, *System Identification: Theory for the User*, Prentice Hall, New York, NY, USA, 1999.
[17] J. Lozoya-Santos, O. Sename, L. Dugard, R. Morales-Menendez, and R. R. Mendoza, "A *LPV* quarter of car with semi-active suspension model including dynamic input saturation," in *Proceedings of the 4th IFAC Symposium on System, Structure and Control*, Ancona, Italy, 2010.
[18] S. M. Savaresi, S. Bittanti, and M. Montiglio, "Identification of semi-physical and black-box non-linear models: the case of *MR*-dampers for vehicles control," *Automatica*, vol. 41, no. 1, pp. 113–127, 2005.
[19] H. S. Lee and S. B. Choi, "Control and response characteristics of a magneto-rheological fluid damper for passenger vehicles," *Journal of Intelligent Material Systems and Structures*, vol. 11, no. 1, pp. 80–87, 2000.
[20] D. Sammier, O. Sename, and L. Dugard, "Skyhook and H_∞ control of semi-active suspensions: some practical aspects," *Vehicle System Dynamics*, vol. 39, no. 4, pp. 279–308, 2003.
[21] C. Boggs, M. Ahmadian, and S. Southward, "Efficient empirical modelling of a high-performance shock absorber for vehicle dynamics studies," *Vehicle System Dynamics*, vol. 48, no. 4, pp. 481–505, 2010.
[22] C. Boggs, L. Borg, J. Ostanek, and M. Ahmadian, "Efficient test procedures for characterizing *MR* dampers," in *Proceedings of the ASME International Mechanical Engineering Congress and Exposition (IMECE '06)*, November 2006.
[23] N. Fukushima, K. Hidaka, and K. Iwata, *Optimum Caracteristics of Automotive Shock Absorbers under Various Driving Conditions and Road Surfaces*, JSAE Review, New York, NY, USA, 1983.
[24] S. M. Savaresi, E. Silani, S. Bittanti, and N. Porciani, "On performance evaluation methods and control strategies for semi-active suspension systems," in *Proceedings of the 42nd IEEE Conference on Decision and Control*, pp. 2264–2269, New York, NY, USA, December 2003.